International Journal of Sustainable Engineering Frontiers
Abbreviated Key Title: Int. J. Sustain. Eng. Front.
ISSN: 3141-6632 (Open Access):
Vol 1: (2): Pp.: 81–104, 2026

Enhancing Thermal Comfort in Humid Tropical Buildings Using Solar Absorption Refrigeration Systems: Case Study of Ebolowa, South-Cameroon

[1,*]Mboumboue, E., [2]Ondoua Belibi, C., [2]Kwefeu Mbakop, F., [3]Goron, D., [4]Wati, E., [3]Chedop, A., [3]Bidias, J. B., & [5]Moungnutou Mfetoum, I.

[1]Environmental Energy Technologies Laboratory/Department of Physics/Faculty of Science/University of Yaoundé 1, P.O. Box: 812 Yaoundé-Cameroon,
[2]Department of Renewable Energy/Higher Institute of Agriculture, Forestry, Water and Environment/University of Ebolowa, P.O. Box: 118, Ebolowa-Cameroon,
[3]Department of Renewable Energy/National Advanced School of Engineering/University of Maroua, P. O. Box 46, Maroua-Cameroon,
[4]Department of Electrical and Electronic Engineering/Faculty of Engineering and Technology/University of Buea, P. O. Box 63, Buea-Cameroon,
[5]Technology and Applied Sciences Laboratory/University Institute of Technology/University of Douala, P.O. Box: 8698, Douala-Cameroon,

*** Corresponding author:** edomboue@gmail.com

Abstract

Amidst climate change and escalating energy demand, thermal comfort in buildings has become a critical concern, particularly in high-temperature regions. The reliance on conventional air conditioners, which are energy-intensive, exacerbates greenhouse gas emissions and electricity consumption. Solar Absorption Refrigeration (SAR) systems emerge as a promising alternative, harnessing solar energy to provide cooling in an environmentally friendly and cost-effective manner. This study focuses on enhancing thermal comfort in buildings through the integration of SAR, aiming to reduce dependence on conventional energy sources and optimize the thermal performance of buildings in humid tropical zones. The specific case of Ebolowa city is examined, with a focus on a test room in the Higher Institute of Agriculture, Forestry, Water and Environment (ISABEE) building. The research seeks to improve thermal comfort by implementing a SAR system in the ISABEE conference room, where a thermal load of 30.32 kW was determined. This assessment led to the design of a SAR system with a capacity of 43.31 kW and a generator pump power of 0.87 kW. The Proportional-Integral-Derivative (PID) controller integrated into the system significantly improved its response time, reducing it from 400 s prior to optimization to 59 s thereafter, thereby ensuring stable thermal comfort despite external temperature variations. A comparison with conventional air-conditioning systems demonstrates that solar refrigeration offers superior long-term cost-effectiveness owing to the substantial energy savings achieved in both residential and commercial applications.

Keywords: *Thermal comfort; humid tropical climate; PID control; exergetic efficiency; SAR; building cooling.*

Accepted 8/5/2026 Int. J. Sustain. Eng. Front. Published: 14/6/2026

Nomenclature:

List of abbreviations and acronyms:

- **BIPV/T** - Building-Integrated Photovoltaic-Thermal
- **CHP** - Combined Heat and Power
- **COP** - Coefficient of Performance
- **COP_{Carnot}** - Carnot Coefficient of Performance
- **F** - Quality factor (COP/COP_{Carnot})
- **H_2O-LiBr** - Water-Lithium Bromide refrigerant-absorbent pair
- **HVAC** - Heating, Ventilating, and Air Conditioning
- **ISABEE** - Higher Institute of Agriculture, Forestry, Water and Environment
- **ISO** - International Organization for Standardization
- **MATLAB** - MATrix LABoratory software environment
- **NH_3** - Ammonia
- **PID** - Proportional-Integral-Derivative (controller)
- **PMV** - Predicted Mean Vote (standard thermal comfort index)
- **SAR** - Solar Absorption Refrigeration system
- **SHE** - Solution Heat Exchanger
- **SHGC** - Solar Heat Gain Coefficient
- **Simulink** - Simulation and Link MATLAB-based simulation environment
- **TRNSYS** - Transient System Simulation Program

Notations:

- ω_n - Natural frequency
- **A** - Surface area (m^2)
- **c_p** - Specific heat of air (J/kg·K)
- **e(t)** - Temperature error signal (T_{set} - T_{room})
- **G** or **I** - Incident solar irradiance (W/m^2)
- **G(s)** - Transfer function (Laplace domain)
- **h** - Specific enthalpy (J/kg)
- **h_{fg}** - Latent heat of vaporization of water (J/kg)
- **K_p**, **K_i**, **K_d** - Proportional, Integral, and Derivative gains of the PID controller
- **$\dot{m}$** - Mass flow rate (kg/s)
- **$\dot{Q}_A$** - Heat rejection in the absorber (W)
- **$\dot{Q}_C$** - Condenser heat rejection (W)
- **$\dot{Q}_E$** - Evaporator cooling capacity (W)
- **$\dot{Q}_G$** - Heat input to the generator (W)
- Q_L - Total latent heat gain (W)
- $Q_{Léquip}$ - Latent heat gain from equipment (W)
- Q_{Loc} - Latent heat gain from occupants (W)
- Q_{Lv} - Latent heat gain due to air exchange or ventilation (W)
- Q_{rs} - Sensible heat gain due to air exchange or ventilation (W)
- Q_S - Total sensible heat gain (W)
- $Q_{sécl}$ - Sensible heat gain from lighting (W)
- $Q_{Séquip}$ - Sensible heat gain from equipment (W)
- Q_{soc} - Sensible heat gain from occupants (W)
- Q_{srRT}- Heat gain by radiation through walls (W)Q_{strT}- Heat transfer through walls (W)
- Q_T – Total cooling load or total heat balance of the room (W)
- s - Complex Laplace variable
- **T** - Absolute Temperature (K or °C)
- **T_0** - Ambient dead-state temperature
- **T_g**, **T_a**, **T_c**, **T_e** - Temperatures of generator, absorber, condenser, and evaporator
- **T_{int}** - Indoor air temperature
- **T_{out}** - Outdoor air temperature
- **T_{set}** - Setpoint temperature
- **U** - Overall thermal transmittance (U-value, $W/m^2·K$)
- **u(t)** - Controller output signal
- **$\dot{V}$** - Volumetric airflow rate (m^3/s)
- **W** - Humidity ratio (kg/kg)
- **$\dot{W}_p$** - Solution pump work (W)
- **x** - LiBr mass fraction in the solution
- **α** - Solar absorptance
- **ε_{SHE}** - Solution Heat Exchanger effectiveness
- **η_{ex}** - Exergetic efficiency
- **ρ** - Air density (kg/m^3)
- ξ - Damping ratio

Units and other common abbreviations:

- **%** - percent
- **°C** - degree Celsius
- **J/(kg·K)** - joule per kilogram-kelvin
- **K** - Kelvin
- **kg/s** - kilogram per second
- **kW** - kilowatt
- **kWh/m²/day** - kilowatt-hour per square meter per day
- **m** - meter
- **m²** - square meter
- **s** - second
- **W** - watt
- **W/(m²·K)** - watt per square meter-kelvin

1. INTRODUCTION

Energy consumption for space cooling is growing faster than any other building end-use, having more than tripled between 1990 and 2016. Largely met by electrically powered fans or air-conditioning systems, this growing demand is making an increasing contribution to

global energy consumption [1]. Conventional vapor-compression air-conditioning systems have been widely utilized due to their capability to maintain stable indoor temperatures [2]. However, they are highly energy-intensive and can increase greenhouse gas emissions, particularly when the electricity mix is dominated by fossil fuels. The decarbonization of the cooling sector can be achieved, *inter alia*, through the adoption of renewable energy-driven cooling systems [3].

Among the various renewable energy sources, solar energy emerges as the most suitable candidate for refrigeration and air-conditioning, given the favorable temporal alignment between maximum cooling demand and peak solar radiation availability [1, 4]. Solar cooling technologies encompass several distinct approaches: solar electric compression refrigeration, solar mechanical compression refrigeration, solar absorption refrigeration, solar adsorption refrigeration, and solar solid desiccant cooling [5]. Among these, SAR systems have garnered considerable attention. It utilizes solar thermal energy, typically collected via solar thermal collectors, to drive a thermodynamic cycle without a mechanical compressor that produces cooling, thereby offering a renewable and low-carbon solution [6].

A wide range of investigations has been undertaken on SAR systems, addressing various aspects of system design and performance. These include experimental studies coupling vapor absorption systems with flat-plate collectors [5, 7, 8], or parabolic trough collectors [9, 10], integrating multi-stage heat storage systems [11, 12], and utilizing binary working fluids. Further research has explored solar-driven hybrid absorption-thermochemical configurations [13, 14], heat pump integration [15], and phase change materials [16–18]. Additionally, numerous numerical simulations have been developed to model and optimize SAR system performance under varying operating conditions [19–23]. Other works have evaluated various refrigerant-absorbent combinations to identify binary systems that offer superior stability and performance under diverse solar radiation intensities. The most common working pairs include water/lithium bromide, ammonia/water, and ammonia/lithium nitrate [24–26]. Ternary systems, such as ammonia/water/lithium bromide and ammonia/lithium nitrate/water, have also been employed by several authors [25, 26].

The integration of SAR systems into buildings requires careful consideration of both the solar collector field and the building's thermal dynamics. Several studies have investigated system configurations and control strategies to optimize performance. Jalalizadeh et al. [27] developed a trigeneration system combining glazed Building-Integrated Photovoltaic-Thermal (BIPV/T) collectors with an absorption chiller using TRNSYS–MATLAB co-simulation, prioritizing solar thermal energy delivery to the absorption cooling system. This solar-driven refrigeration approach reduced building cooling demand by 36%, with the overall system meeting 29% of annual building energy requirements. Similarly, Shirazi et al. [28] used TRNSYS simulations to optimize a solar-assisted absorption chiller system for a building, comparing control strategies and auxiliary heater configurations to achieve up to a 20% higher solar fraction without substantial additional cost.

The performance of SAR systems has been evaluated across diverse climatic conditions. Using TRNSYS simulations, Noferesti et al. [29] investigated a solar-assisted absorption chiller system for a high-cooling-load building in southeast Iran. The solar absorption system achieved indoor temperature improvements of up to 3.08 °C and reduced power consumption by up to 84% compared to the existing cooling system, with evacuated tube collectors providing the best performance. Reda et al. [30] used TRNSYS dynamic simulations to investigate two configurations of a solar-driven absorption cooling system for an office building in Finland's cold climate. Results showed that directly connecting solar collectors to the chiller outperformed tank-only supply, particularly under low irradiance, demonstrating the technology's potential to reduce cooling energy consumption and enable combined heat and power (CHP) plant operation during summer months.

Beyond system configuration and climatic adaptability, several studies have employed thermodynamic analyses to identify efficiency improvements. Aman et al. [31] developed a thermodynamic model incorporating energy and exergy analyses of a 10 kW solar-driven ammonia-water absorption chiller for residential air-conditioning. Results revealed that the absorber accounts for 63% of total exergy loss, followed by the generator (13%) and condenser (11%), with exergy losses in the condenser and absorber being most sensitive to temperature increases. A comprehensive thermodynamic modeling of a solar-powered lithium bromide-water absorption refrigeration system was conducted by Kerme et al. [32]. They analyzed collector type, generator temperature, and heat exchanger effectiveness through energy and exergy analyses. Results showed that evacuated tube collectors achieved the highest efficiency, while exergy analysis revealed the solar collector as the primary source of exergy destruction, accounting for 71.9% of input exergy and 84% of total losses, with an overall system improvement potential of 84.7%.

Together, these studies demonstrate that SAR systems' performance is influenced by multiple factors, including system configuration, control strategy, climatic conditions, and component-level thermodynamic inefficiencies, highlighting the need for integrated design approaches tailored to specific applications and locations. However, performance in humid tropical climates, characterized by high latent loads, persistent outdoor heat, and strong seasonal variability, remains less documented. This gap is particularly important in regions such as Ebolowa, where buildings experience high cooling demand, significant moisture loads, and solar

conditions that may support solar-driven cooling if the system is properly sized and controlled.

Although numerous studies have examined SAR systems, most have focused on component performance, thermodynamic optimization, or building cooling potential under temperate, subtropical, or generalized hot climates. In contrast, limited attention has been given to the dynamic integration of SAR with the thermal behavior of a real building in a humid tropical environment, where latent loads, high outdoor temperatures, and solar variability strongly influence indoor comfort. The novelty of this study lies in developing and applying a coupled SAR-building model for a real conference room in Ebolowa, South-Cameroon, combining cooling-load assessment, absorption chiller sizing, exergy analysis, and PID-based temperature regulation within a single framework. This integrated approach goes beyond conventional SAR performance studies by explicitly evaluating not only whether solar cooling can meet the building load, but also how control action improves transient response and thermal stability under local climatic conditions.

This study aims to present a comprehensive methodology and analysis for a SAR system tailored to a real conference room in Ebolowa, South-Cameroon, a representative humid tropical location. The specific objectives are: (1) to conduct a detailed thermal load assessment of the space using a simplified method accounting for all significant heat gains; (2) to model a single-effect H_2O-LiBr absorption chiller and size the required solar thermal array; (3) to develop a dynamic model of the coupled building and cooling system and implement a proportional-integral-derivative (PID) controller for temperature regulation; and (4) to simulate and analyze the system's energy, exergy, and control performance using MATLAB/Simulink. Accordingly, this paper addresses the following research questions: Can SAR satisfy the cooling demand of a humid tropical building? What improvement in thermal response is achieved using PID control? What are the energy and thermodynamic performance indicators of the proposed system?

This paper is structured into four main sections that follow a logical progression from problem framing to methodological development and, finally, to performance assessment and conclusions. After the introduction, Section 2 presents the general methodology conducting the study, including the system description and the mathematical modeling of the single-effect H_2O-LiBr absorption cycle. Section 3 reports and discusses the results, first detailing the thermal load breakdown and the key design parameters of the SAR system, then analyzing the exergetic efficiency of the chiller, and finally comparing the dynamic response of the system with and without PID control, illustrating the significant improvement in response time and stability. The paper concludes in Section 4 by summarizing the findings, highlighting the technical feasibility and energy efficiency advantages of the solar-driven solution in a humid tropical context, and outlining the potential of such systems for thermal comfort enhancement in Cameroon and similar regions.

2. METHODOLOGY

2.1. Site, data and system description

2.1.1. Study site

Ebolowa (2.93°N, 11.15°E, altitude 620 m) is a city in Central Africa, located in the southern part of Cameroon. It lies slightly north of the Equator, within a humid tropical zone characterized by warm temperatures, abundant rainfall, and high solar availability throughout the year. Figure 1 below presents the building and the conference room under study.

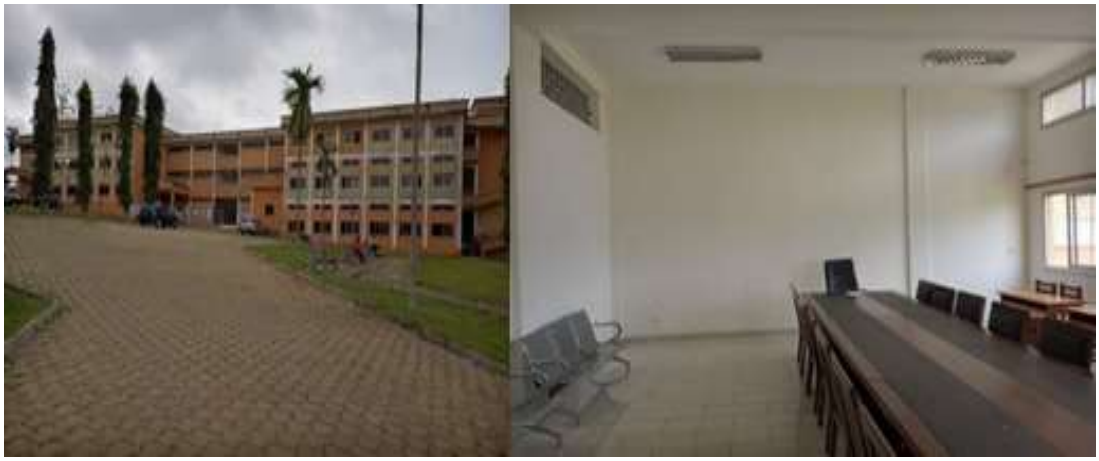

Figure 1: *ISABEE's building and conference room under study*

1.1.1. Data acquisition

Weather data supporting the study were obtained from a local climate centre for Ebolowa and used to extract the monthly solar irradiation and outdoor temperature values representative of the site. These data were selected because they reflect the humid tropical climate of the location and capture the conditions most relevant to system sizing, especially the warm design hour and the periods of high solar availability that drive the absorption cooling system. They therefore represent design conditions because they correspond to the climatic loads that the system must withstand under worst-case or near-worst-case operating scenarios, rather than to short-term average conditions.

Ebolowa in southern Cameroon exhibits a humid tropical climate. Key design data include an annual average solar irradiation of 4.48 kWh/m²/day and design outdoor conditions of 30 °C dry-bulb temperature with 65% relative humidity. Its climate makes it a representative site for studying building cooling needs and renewable-energy-based refrigeration solution, especially for applications where both sensible and latent loads are important. The monthly variation of temperature and solar radiation, which are critical for system simulation, are shown in Figure 2 and Table 1, respectively.

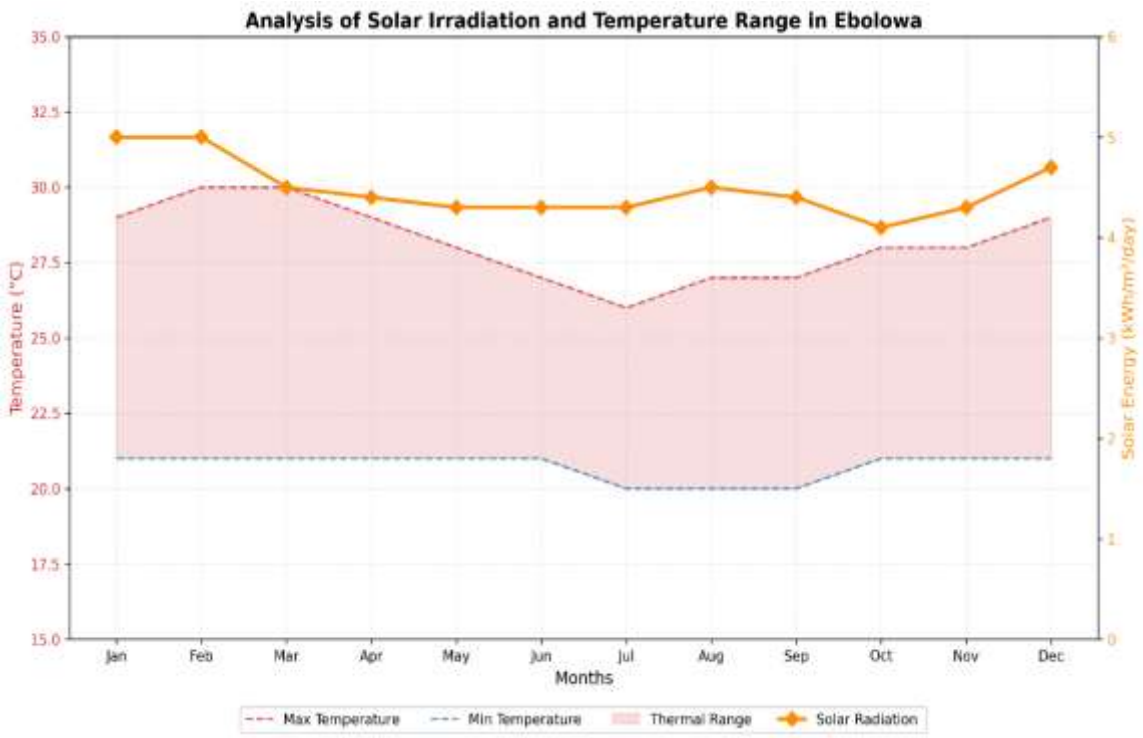

Figure 2: *Monthly evolution of temperature and solar radiation at Ebolowa*

Table 1: *Solar irradiation in Ebolowa*

Months	Jan	Feb	Mar	Apr	Mai	Jun	Jul	Aug	Sep	Oct	Nov	Dec
Solar radiation (kWh/m²/day)	5.0	5.0	4.5	4.4	4.3	4.3	4.3	4.5	4.4	4.1	4.3	4.7

The main model inputs used for sizing and simulation are summarized in table 2, while the building envelope parameters and collector specifications should be reported explicitly to improve reproducibility.

Table 2: *Model inputs*

Parameter	Symbol / Description	Value	Unit	Notes
Collector efficiency	η_{coll}	0.50	–	Assumed average efficiency for evacuated tube collectors.
COP assumption	COP	0.70	–	Used for sizing the absorption chiller from the design cooling load.
Indoor setpoint temperature	T_{set}	19	°C	Target comfort temperature for the conference room.
Outdoor design temperature	T_{out}	30	°C	Design ambient condition used for load estimation.
Outdoor relative humidity	RH	65	%	Design humid tropical condition for Ebolowa.
Building envelope U-value	U	1.2 (Walls); 0.8 (Roof); 3.5 (Glazing)	W/m²·K	Use the wall, roof, and glazing values reported in the building description.
Heat transfer coefficients	h	3 (Indoor); 12 (Outdoor)	W/m²·K	Include indoor and outdoor convective coefficients used in the load model.
Collector specification	Type	Evacuated tube collectors	–	Solar thermal collectors used to supply the generator.
Collector design irradiance	G_{design}	1000	W/m²	Used for collector sizing.
Collector area	A_{coll}	86.62	m²	Required aperture area for the design case.
Number of collectors	N	44	panels	Based on the chosen collector module size.
Generator thermal input	Q_G	43.31	kW	Thermal power required by the chiller.
Pump power	P_{pump}	0.87	kW	Estimated as a small fraction of generator heat input.

1.1.2. System description

The proposed system replaces the conventional electrically driven vapor-compression cycle with a thermally driven single-effect absorption cycle using a binary solution of water as the refrigerant and lithium bromide (LiBr) as the absorbent. The basic layout comprises the following main components: a generator, a condenser, an evaporator, an absorber, a solution heat exchanger, a solution pump, and expansion devices. Solar thermal energy, collected by evacuated tube collectors, supplies the heat input ($\dot{Q}_G$) to the generator. This heat induces the desorption of refrigerant vapor (water) from the rich LiBr solution. The vapor flows to the condenser, where it rejects heat ($\dot{Q}_C$) and condenses. The liquid refrigerant then expands through a throttle valve into the low-pressure evaporator, where it extracts heat ($\dot{Q}_E$) from the building's chilled water loop, thereby producing the cooling effect. The resulting vapor is absorbed by the weak LiBr solution in the absorber, releasing heat ($\dot{Q}_A$), and the regenerated strong solution is pumped back to the generator, completing the cycle. A basic schematic of an absorption refrigeration system is shown in Figure 3 [33].

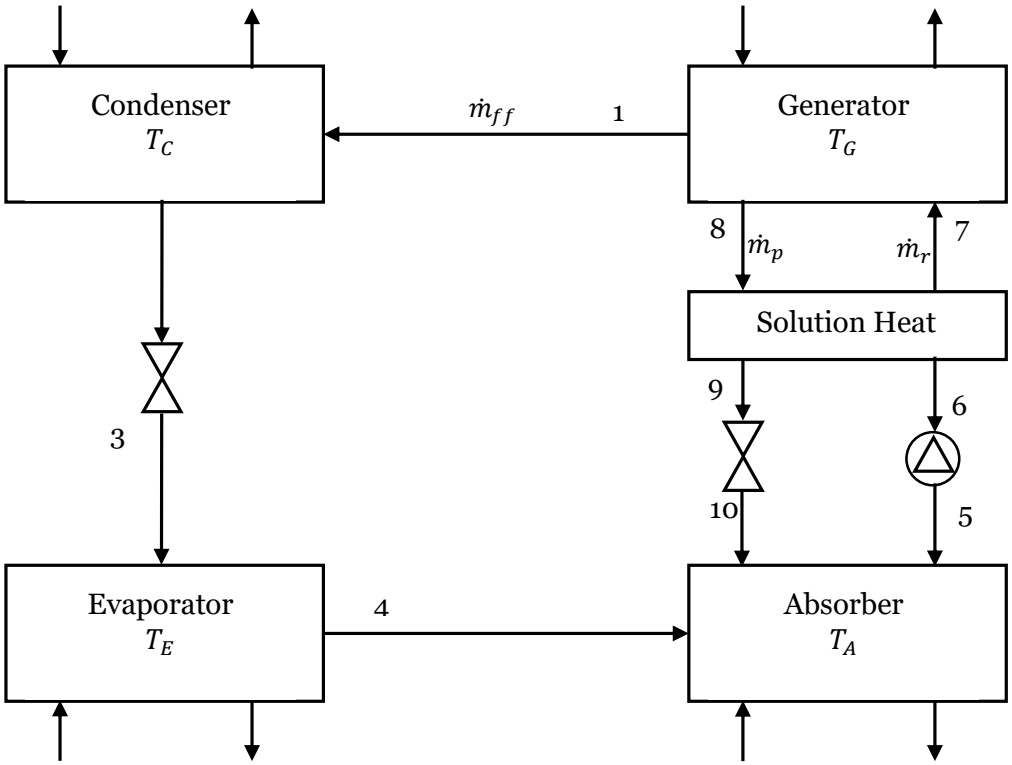

Figure 3: *Basic schematic of an absorption refrigeration system.*

1.2. Mathematical modeling of the absorption cycle

The modeling of the absorption cycle is based on the application of mass and energy conservation principles to each component under steady-state conditions. The following standard assumptions are adopted to simplify the analysis while preserving the essential physics: i) pressure drops are negligible, ii) expansion through the valves is isenthalpic, iii) changes in kinetic and potential energy are insignificant, iv) the system is adiabatic (no heat loss to the surroundings), and v) the solution leaving the generator and absorber is saturated.

The modeling assumptions are justified because the study focusses on the design-point performance of a single-effect H_2O-LiBr absorption system under representative operating conditions rather than on detailed transient fluid dynamics. The steady-state assumption is appropriate since the main objective is to estimate cooling capacity, COP, and exergy performance at nominal conditions, where variations over time are slow compared with the component balance calculations. Negligible pressure drops can also be assumed because the system is analyzed at the component level, and the piping and heat exchangers are designed to minimize hydraulic losses relative to the dominant pressure levels in the generator, condenser, evaporator and absorber. Likewise, assuming adiabatic components is reasonable for a first-order thermodynamic model because external heat losses are small compared with the large heat transfers occurring in the generator, absorber, and condenser, especially when the equipment is properly insulated. These assumptions simplify the analysis while preserving the main physical behavior of the cycle and are commonly adopted in preliminary absorption-chiller modeling.

1.2.1. Mass balances

The overall mass balance for the solution stream at the generator, where the refrigerant separates, is given by Eq. (1).

$$\dot{m}_r = \dot{m}_{ff} + \dot{m}_p \quad (1)$$

Where $\dot{m}_r$ is the mass flow rate of the rich solution entering the generator, $\dot{m}_{ff}$ is the mass flow rate of the pure refrigerant vapor, and $\dot{m}_p$ is the mass flow rate of the weak (poor) solution leaving the generator. The conservation of the LiBr mass, which is non-volatile and remains entirely in the liquid solution, is expressed by Eq. (2).

$$\dot{m}_r x_r = \dot{m}_p x_p \quad (2)$$

Here, x_r and x_p represent the mass fractions of LiBr in the rich and poor (weak) solutions, respectively. By solving Eqs. (1) and (2) simultaneously, the individual solution flow rates can be expressed in terms of the refrigerant flow rate and concentrations, as shown in Eqs. (3) and (4):

$$\dot{m}_r = \frac{x_p}{x_p - x_r}\dot{m}_{ff} \quad (3)$$

$$\dot{m}_p = \frac{x_r}{x_p - x_r}\dot{m}_{ff} \quad (4)$$

These relationships are fundamental for sizing system components and calculating energy transfers.

1.2.2. Component energy balances

The steady-flow energy equation is expressed by Eq. (5):

$$\sum \dot{m}_{in} h_{in} - \sum \dot{m}_{out} h_{out} + \dot{Q} = 0 \quad (5)$$

Applying it to each component yields the following governing equations. For the absorber, where refrigerant vapor is absorbed into the weak solution, releasing heat to a cooling tower loop, the energy balance is given by Eq. (6):

$$\dot{Q}_A = \dot{m}_{ff} h_4 + \dot{m}_p h_{10} - \dot{m}_r h_5 \quad (6)$$

Where h_4, h_{10} and h_5 are the specific enthalpies of the refrigerant vapor from the evaporator, the weak solution entering, and the rich solution leaving the absorber, respectively. $\dot{Q}_A$ is the heat rejection rate from the absorber. The solution pump work, typically small but non-negligible, is calculated from the isentropic compression of the liquid solution:

$$\dot{W}_{POM} = \dot{m}_r(h_6 + h_5) \quad (7)$$

The Solution Heat Exchanger (SHE) improves cycle efficiency by preheating the rich solution entering the generator using the hot weak solution leaving it. Its effectiveness is defined as:

$$\varepsilon_{SHE} = \frac{T_9 - T_8}{T_6 - T_8} \quad (8)$$

The energy balance across the SHE is given by Eq. (9).

$$\dot{m}_r(h_1 - h_6) = \dot{m}_p(h_8 - h_5) \quad (9)$$

The refrigerant is separated from the solution by heat supplied to the generator from an external thermal source. The energy balance is:

$$\dot{Q}_G = \dot{m}_{ff} h_1 + \dot{m}_p h_8 - \dot{m}_r h_7 \quad (10)$$

Here, h_1 is the enthalpy of the superheated refrigerant vapor, and h_7 and h_8 are the enthalpies of the strong and weak solution streams, respectively. The weak refrigerant solution exits the generator and undergoes an isenthalpic expansion through a valve; therefore $h_9 = h_{10}$. The condenser heat rejection is given by Eq. (11).

$$\dot{Q}_C = \dot{m}_{ff}(h_1 - h_2) \quad (11)$$

Assuming isenthalpic expansion, one can write:

$$h_3 = h_2 \quad (12)$$

Finally, the evaporator provides the useful cooling effect by absorbing heat for refrigerant evaporation:

$$\dot{Q}_E = \dot{m}_{ff}(h_4 - h_3) \quad (13)$$

The enthalpy values at each state point h_1, h_2, ... are determined from property correlations for the H_2O-LiBr solution and pure water/steam, often implemented via functions or look-up tables in simulation environments [34].

1.2.3. Performance parameters

The primary performance metric is the Coefficient of Performance (COP), defined as the ratio of the cooling effect to the primary energy input (thermal energy supplied to the generator plus pump work).

$$COP_{cycle} = \frac{\dot{Q}_E}{\dot{Q}_G + \dot{W}_{POM}} \quad (14)$$

To evaluate the thermodynamic perfection of the cycle, the Carnot COP serves as the theoretical maximum for the given temperature reservoirs:

$$COP_{carnot} = \left(\frac{T_G - T_A}{T_G}\right)\left(\frac{T_E}{T_C - T_E}\right) \quad (15)$$

Where T_G, T_A, T_C and T_E are the absolute temperatures of the generator, absorber, condenser, and evaporator, respectively. The quality factor F_q compares the actual performance to the ideal.

$$F_q = \frac{COP_{cycle}}{COP_{Carnot}} \quad (16)$$

A more rigorous thermodynamic assessment is provided by exergetic efficiency η_{ex}, which quantifies the effective

utilization of the input exergy. For the absorption chiller, it is expressed as:

$$\eta_{ex} = \frac{\dot{Q}_E\left(\frac{T_0}{T_{SE}}-1\right)}{\dot{Q}_G\left(1-\frac{T_0}{T_{SG}}\right)+\dot{W}_P} \quad (17)$$

Where T_0 is the dead-state (ambient) temperature, T_{SE} and T_{SG} are the average temperatures of heat reception in the evaporator and heat supply in the generator, respectively.

2.3. Thermal load assessment of the conference room

The sizing of the cooling system necessitates a detailed calculation of the building's cooling load. The methodology, summarized in the flowchart of Figure 4, follows the classical heat balance method, accounting for all sensible and latent heat gains during the design hour.

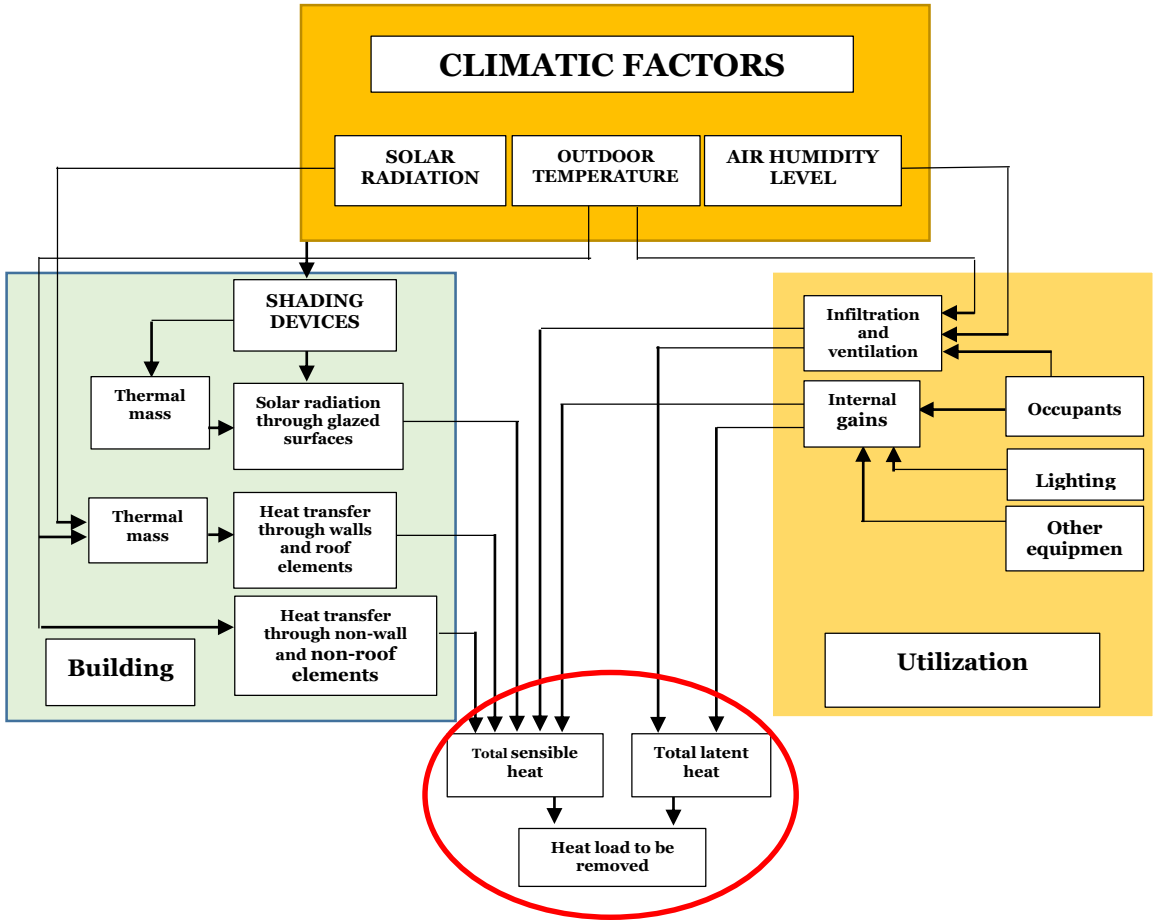

Figure 4: *Flowchart for building's thermal load assessment*

1.2.4. External loads

External loads originate from heat transfer through the building envelope due to temperature differences and solar radiation. Conductive/convective heat transfer through opaque walls, the roof, and glazing is calculated using Eq. (18):

$$Q_{Str} = k.S.\Delta\theta \quad (18)$$

Where k is the overall thermal transmittance (U-value) of the surface (W/m²·K), S is the surface area (m²), and $\Delta\theta$ is the temperature difference between indoor and outdoor design conditions (°C).

Solar heat gain through opaque walls considers absorbed solar radiation that is subsequently conducted inward:

$$Q_{Srm} = \alpha.F.S.R_m \quad (19)$$

Where α is the solar absorptance of the outer surface, F is the solar radiation factor (fraction transmitted inward), and R_m is the incident solar irradiance on the wall (W/m²). Solar heat gain through windows is a major contributor in tropical climates. For glazing, it is computed as:

$$Q_{Srv} = \alpha.g.S/R_v \quad (20)$$

Where g is the solar heat gain coefficient (SHGC) of the glazing system, and R_v is the incident solar irradiance. Air renewal in an air-conditioned space is necessary for hygienic reasons. It is generally achieved through ventilation (natural or mechanical) and infiltration, which introduces outdoor air into the conditioned space. This process contributes both sensible Q_{Sr} and latent Q_{Lv} heat loads to the room.

$$Q_{Sr} = q_v.(\theta_e - \theta_i).c_p.\rho \quad (21)$$

$$Q_{Lv} = q_v(\omega_e - \omega_i).h_{fg} \quad (22)$$

With q_v being the volumetric airflow rate (m³/s), θ the dry-bulb temperature (°C), ω the humidity ratio (kgwater/kgdry air), c_p the specific heat of air, ρ the air density, and h_{fg} the latent heat of vaporization of water.

1.2.5. Internal loads

Internal loads are generated within the conditioned space. Occupants release sensible Q_{Soc} and latent heat Q_{Loc} depending on their activity level.

$$Q_{Soc} = n.C_{Soc} \quad (23)$$

$$Q_{Loc} = n.C_{Loc} \quad (24)$$

Where C_{Soc} and C_{Loc} are sensible and latent heat emission rates per person. Lighting and electrical equipment contribute sensible heat. For lighting:

$$Q_{Secl} = P_{installed}.F_{use}.F_{allowance} \quad (25)$$

Where $P_{installed}$ is the total installed power, F_{use} is the usage factor, and $F_{allowance}$ accounts for ballast losses: 1.25 for fluorescent lamps and 1 for incandescent lamp.

1.2.6. Total cooling load

The total sensible Q_S and latent Q_L loads are summed from all contributions:

$$Q_S = Q_{Str} + Q_{Srm} + Q_{Srv} + Q_{Sr} + Q_{Soc} + Q_{Secl} + Q_{Sequip} \quad (26)$$

$$Q_L = Q_{Lr} + Q_{Loc} + Q_{Lequip} \quad (27)$$

The total cooling load Q_T is:

$$Q_T = Q_S + Q_L \quad (28)$$

Where:

Q_{strT}- Heat transfer through walls (W)

Q_{srRT}- Heat gain by radiation through walls (W)

Q_{rs} - Sensible heat gain due to air exchange or ventilation (W)

Q_{Lv} - Latent heat gain due to air exchange or ventilation (W)

Q_{soc} - Sensible heat gain from occupants (W)

Q_{Loc} - Latent heat gain from occupants (W)

$Q_{sécl}$ - Sensible heat gain from lighting (W)

$Q_{Séquip}$ - Sensible heat gain from equipment (W)

$Q_{Léquip}$ - Latent heat gain from equipment (W)

Q_S - Total sensible heat gain (W)

Q_L - Total latent heat gain (W)

Q_T – Total cooling load or total heat balance of the room (W)

A safety factor of 5% is added to account for uncertainties, yielding the design cooling capacity ϕ_0:

$$\phi_0 = Q_T(1 + s_f) \quad (29)$$

2.4. System sizing procedure

Based on the calculated design load Q_T and assuming a typical COP for a single-effect H_2O-LiBr chiller, the required thermal power input to the generator is approximately 43.33 kW. The generator solution pump power is estimated as a small percentage (2%) of Q_G:

$$P_{pump} = 0.02 \times Q_G \quad (30)$$

The required aperture area of solar thermal collectors is determined by balancing the generator demand with the available solar energy:

$$A_{coll} = \frac{Q_G}{G_{design} \times \eta_{coll}} \quad (31)$$

Assuming a design irradiance $G_{design} = 1000$ and an average collector efficiency $\eta_{coll} = 0.5$ for evacuated tubes, the area is $A_{coll} = 86.62\ m^2$.

2.5. Dynamic modeling of building-system coupling and PID control

To simulate transient performance, a dynamic model coupling the room's thermal mass with the cooling system was developed. The rate of change of room temperature is governed by a heat balance on the room air mass:

$$M_{air}c_p \frac{dT_{roon}}{dt} = \dot{Q}_{gain} - \dot{Q}_{cool} \quad (32)$$

Where $\dot{Q}_{gain}$ represents the net heat gain from external and internal sources (simplified here as a function of T_{tout}), and $\dot{Q}_{coll}$ is the cooling rate supplied by the SAR system's fan coil unit. Assuming the cooling power is proportional to an air flow rate $\dot{M}$ and the temperature difference between supply air T_{cold} and room air T_{room}, and that heat loss is driven by the overall

building envelope conductance UA_{env}, Eq. (33) can be expanded to:

$$\frac{dT_{room}}{dt} = \frac{1}{M_{air}c_p}\left[\dot{M}.c_p(T_{cold} - T_{room}) - UA_{env}(T_{room} - T_{out})\right] \quad (33)$$

To maintain the room temperature at a desired setpoint T_{set}, a PID controller is implemented. The controller adjusts the cooling capacity (e.g., by modulating a valve or pump speed) based on the error $e(t) = T_{set} - T_{room}(t)$. The standard PID control law is:

$$u(t) = K_p.e(t) + K_i\int_0^t e(\tau)d\tau + K_d\frac{d}{dt}(e(t)) \quad (34)$$

The controller parameters K_p, K_i and K_d were tuned using the Ziegler-Nichols method [35]. Initially, the integral and derivative gains were set to zero, and K_p was increased until sustained oscillations were observed at the ultimate gain $K_u = 10$ with an oscillation period $T_u = 80$. Parameter τ is time constant. The PID parameters were then calculated as [35]:

$K_p = 0.6K_u = 6$, $K_i = \frac{2K_P}{T_u} = 0.15$, $K_d = \frac{K_pT_u}{8} = 60$

These values were further refined empirically in simulation to achieve a fast, stable response with minimal overshoot.

2.6. Simulation environment

The complete system, comprising the absorption cycle model, the building thermal model, the solar thermal collector and the PID controller was implemented in MATLAB/Simulink. The absorption cycle was modelled using the governing equations (Eqs. 1-17) coupled with property functions. The building model was based on Eq. 33, and the PID controller on Eq. 34. Simulations were conducted under various outdoor temperature scenarios to evaluate system performance with and without the controller.

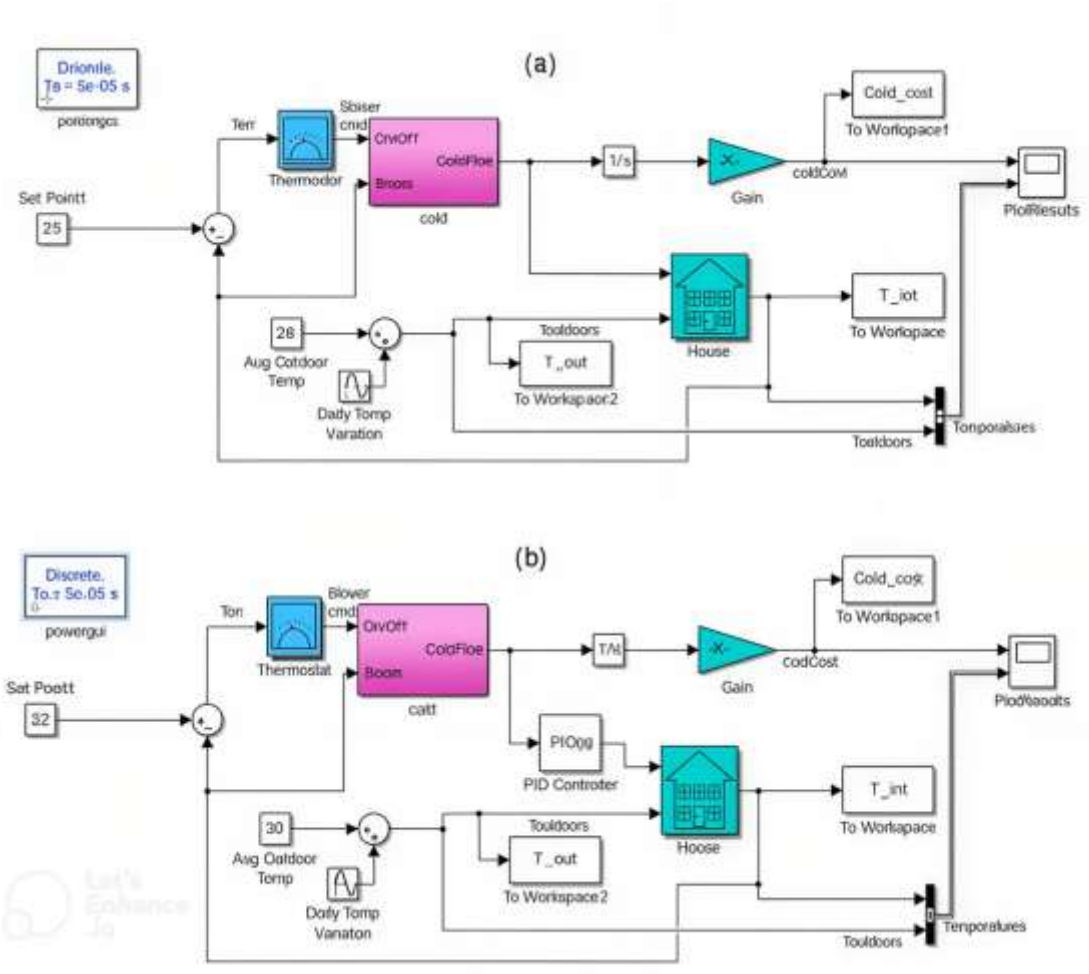

Figure 5: *Diagram of the Absorption Refrigeration System without PID (a) and with PID (b)*

Figure 5a presents the complete Simulink model of the absorption refrigeration system integrated with the conference room thermal model. This diagram visually represents the complex interactions between the chiller components, the building envelope, and environmental inputs, serving as the computational foundation for all subsequent simulations. Figure 5b shows the enhanced system architecture incorporating the PID controller. The controller actively adjusts system parameters based on the error between the measured and desired temperatures, enabling dynamic optimization of the cooling output.

3. RESULTS AND DISCUSSION

3.1. Thermal load assessment

Table 3 presents a comprehensive breakdown of the thermal contributions within the ISABEE conference room. The total cooling load of 30.32 kW validates the requirement for a substantial cooling system. Notably, solar radiation through the walls (9.57 kW) and the latent heat from ventilation (5.44 kW) emerge as the dominant contributors, which is characteristic of the humid tropical climate. This detailed breakdown confirms that both sensible and latent loads must be addressed to ensure effective thermal comfort, thereby supporting the selection of an absorption system capable of managing high latent loads through adequate dehumidification.

Table 3*: Thermal balance of the conference room.*

N°	Heat flows		Values (W)
01	Heat transfer through walls (Q_{strT})		957,712 W
02	Heat gain by radiation through walls (Q_{srRT})		6794.35 W
03	Heat gain through air exchange in the case of natural ventilation	Sensible heat flow (Qrs)	1425.60 W
		latent heat flow (Q_{Lv})	5443.20 W
04	Heat input from occupants	Sensible heat flow (Q_{soc})	4020.00 W
		Latent heat flow (Q_{Loc})	2940.00 W
05	Heat input from lighting: fluorescent light is used ($Q_{sécl}$)		64.00 W
06	Heat input from equipment	Sensible heat flow ($Q_{Séquip}$)	5630 W
		Latent heat flow ($Q_{Léquip}$)	225 W
07	Total sensible heat (Q_S)		18891.16 W
08	Total latent heat flow (Q_L)		8608.20 W
Total heat balance or cooling capacity of the system (Q_T)			30318 W

.2. System parameters

Table 4 summarizes the key design parameters derived from the thermal load analysis. The absorption chiller requires a significant thermal input of 43.31 kW, which dictates the sizing of the solar thermal array. The pump power (0.87 kW) represents only approximately 2% of the thermal input, highlighting the energy efficiency advantage of thermally driven systems over electrically driven compressors. The calculated collector area (86.62 m²) and the resulting 44 panels provide a concrete basis for system implementation, demonstrating the feasibility of meeting cooling demands with solar energy at this location.

Table 4*: Parameters of the solar Absorption refrigeration system*

N°	Designation	Values
01	The power required for the absorption refrigeration (w)	43.31 kW
02	Generator pump power ($P_{pump\ in}$ W)	0.87 kW
03	The surface area of solar thermal collectors (m²)	86.62 m²
04	The number of solar thermal panels to be installed	44

1.3. Exergetic efficiency curve of the absorption machine

The curve of Figure 6 indicates that exergetic efficiency remains within a reasonable range across different generator temperatures, demonstrating good thermodynamic quality for a single-effect system. This performance aligns with literature values for similar H_2O-LiBr chillers, confirming that the system design avoids significant irreversibilities and operates near its theoretical optimum for the given temperature lifts between the heat source and sink.

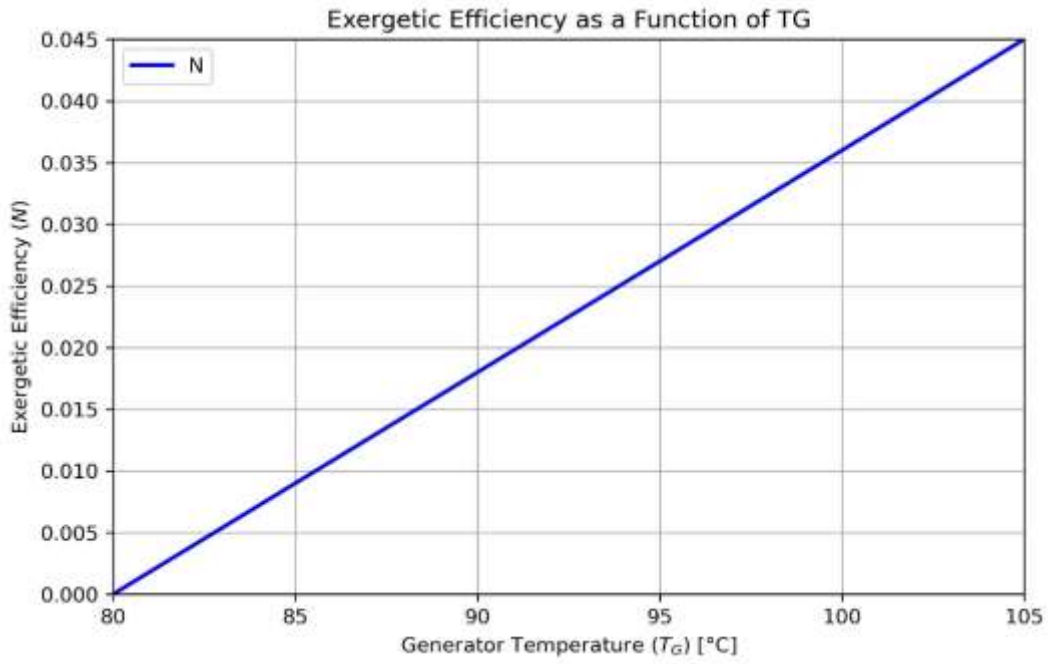

Figure 6: *Exergetic efficiency curve*

The exergetic efficiency curve in figure 6 indicates that the proposed H_2O-LiBr absorption chiller operates within a realistic performance range for a single-effect solar-driven system. From the simulation, the exergetic efficiency varies approximately between 0.20 and 0.35 over the investigated generator temperature range, with a maximum value close to 0.35 obtained near the optimum operating condition. This result is consistent with the literature: Al-Tahaineh [36] reported maximum exergetic efficiency values of about 0.36 for a 10 kW solar-assisted H_2O-LiBr absorption chiller, while other exergy analyses of LiBr-H_2O systems indicate that performance of the range of 0.20-0.35 is typical for single-effect configurations under practical operating conditions [37]. The comparison confirms that the present system is thermodynamically credible and that its performance is comparable to previously published solar absorption cooling systems, while still leaving room for improvement through better heat-source matching, reduced temperature lifts, and enhanced heat exchanger effectiveness [38]. Table 5 compares these values with those reported in the literature. The literature values are drawn from a recent 10 kW H_2O-LiBr solar-driven absorption chiller study and from broader LiBr-H_2O exergy analyses [36, 39].

Table 5: *Comparison with previous studies*

Study	**System type**	**COP**	**Exergetic efficiency/ECOP**	**Main note**
Present study	Single-effect H_2O-LiBr SAR system for Ebolowa conference room	0.70	0.20-0.35, peak close to 0.35	Fits a humid tropical building case and includes PID control
Al-Tahaineh [36]	10 kW simple H_2O-LiBr solar absorption chiller	0.75-0.81	0.342-0.36	Maximum values obtained near a desorber temperature of about 90 °C
J. Zheng et al. [39]	Absorption cooling/heating system	Not stated in snippet	Exergy analysis performed	Confirms that LiBr-H_2O performance depends strongly on operating temperature and heat-source conditions.

The comparison shows that the present system operates within the performance range reported in the literature for single-effect LiBr-H_2O solar absorption chillers, indicating that the modeled design is thermodynamically credible.

1.4. System performance without and with PID

Figures 7-9 demonstrate the system's dynamic response under three different operating scenarios without PID control. The parameters considered are the indoor temperatureT_{int}, the outdoor temperature T_{out}, and the cooling flow cost or gain. In all three cases, the response time is notably long, approximately 450 s, for both the cooling flow gain and the indoor temperature, whereas the outdoor temperature remains variable. Following this extended response period, the cooling flow gain and indoor temperature stabilize and remain constant during operation. Given this significant delay, an alternative system design incorporating a PID controller was proposed to overcome this limitation.

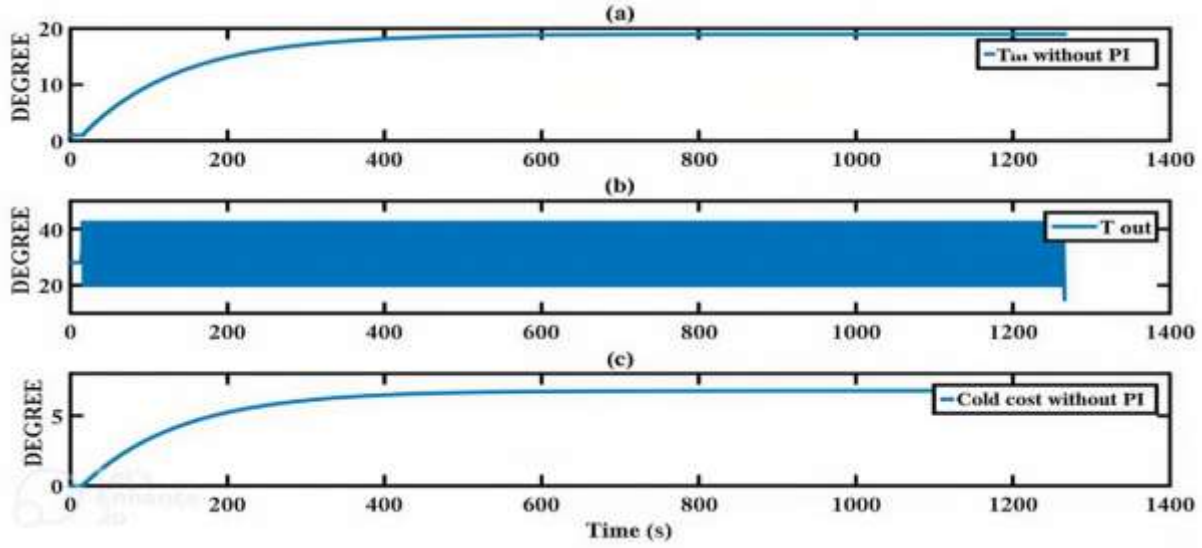

Figure 7: *Experience 1 [25 °C, 28 °C, 19 °C]*

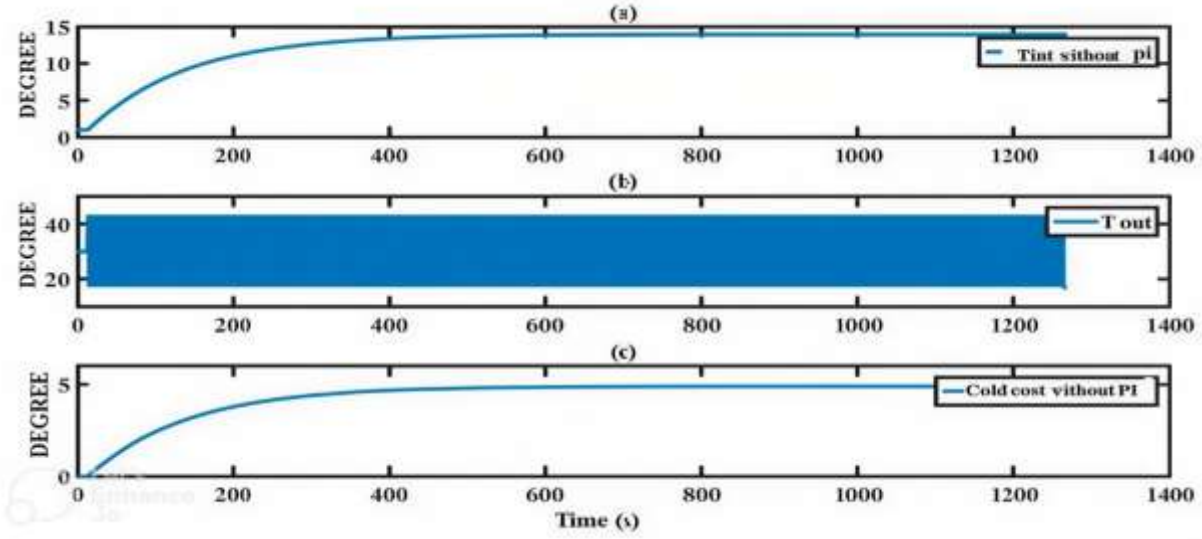

Figure 8: *Experience 2 [30 °C, 32 °C, 16 °C]*

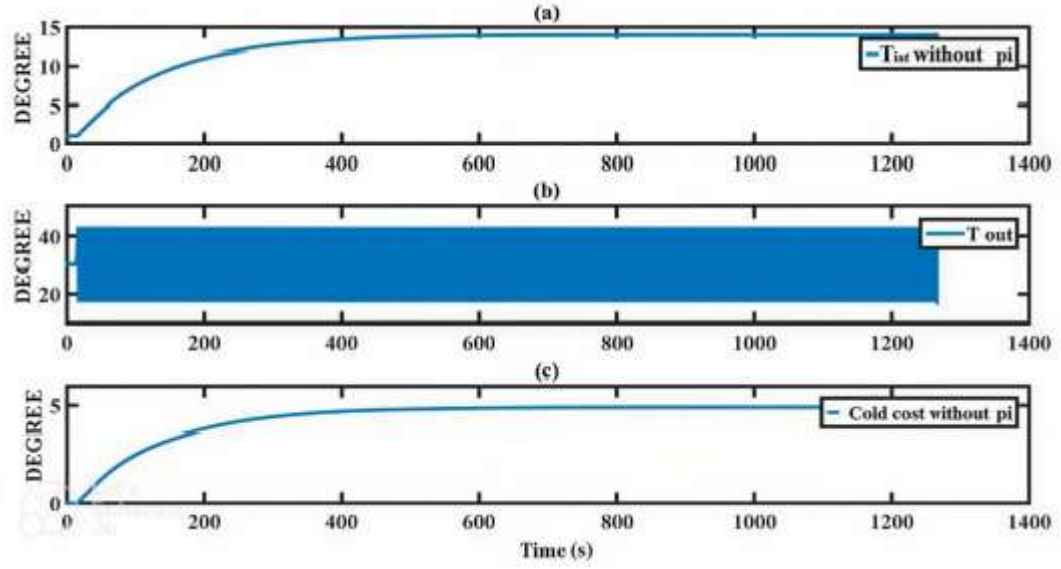

Figure 9: *Experience 3 [32 °C, 30 °C, 14 °C]*

The results for the system with PID control are depicted in Figures 10-12. Here, the response time for the cooling flow gain is reduced to effectively zero seconds, while that for the indoor temperature becomes very fast, even as the outdoor temperature remains variable. The three parameters studied remain constant following the system's rapid response.

In a second stage of observation, the response time is noted to have improved considerably, thereby enabling effective system regulation. Coupling an absorption refrigeration system with a PID controller enhances process control and stability by dynamically adjusting system parameters in real time. The PID controller influences the system through temperature regulation, cycle efficiency improvement, fluctuation reduction, system pressure management, optimization of cycle state transitions, and operating cost reduction.

In summary, coupling a PID controller with an absorption refrigeration system improves system stability, maximizes energy efficiency, and reduces operating costs by dynamically and precisely adjusting system parameters.

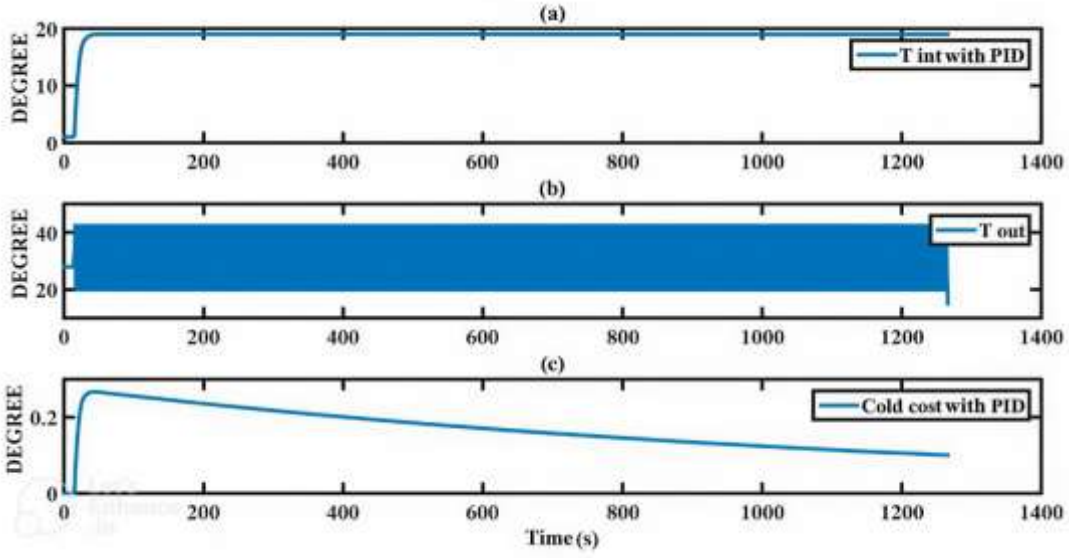

Figure 10: *Experience 4 [25 °C, 28 °C, 19 °C]*

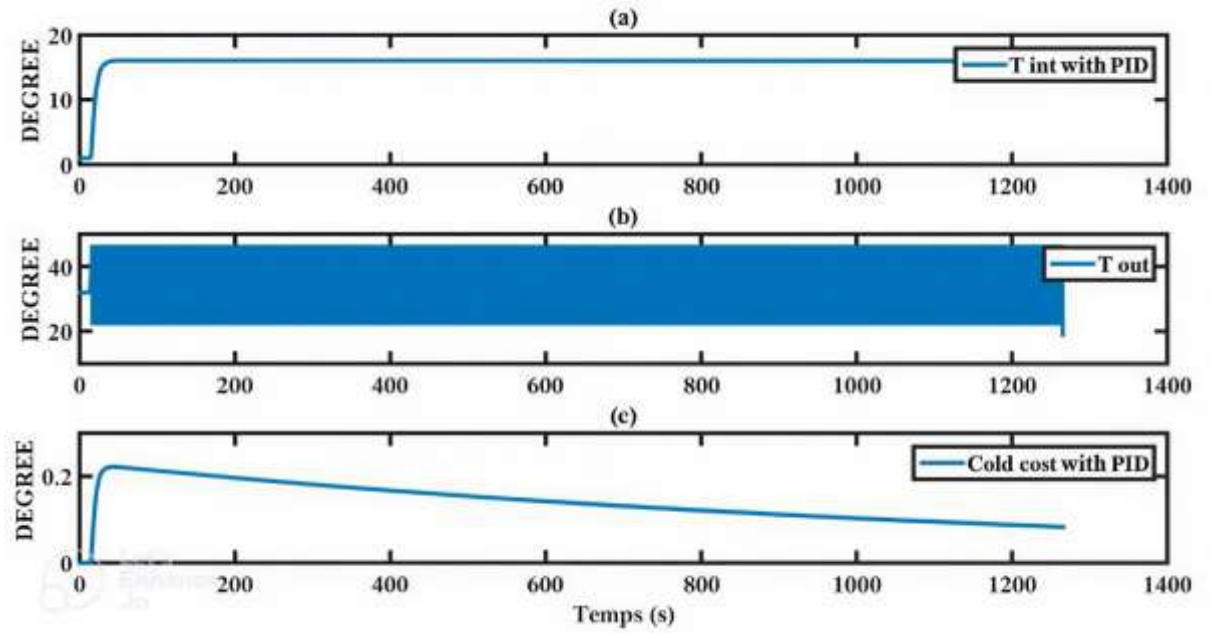

Figure 11: *Experience 5 [30 °C, 32 °C, 16 °C]*

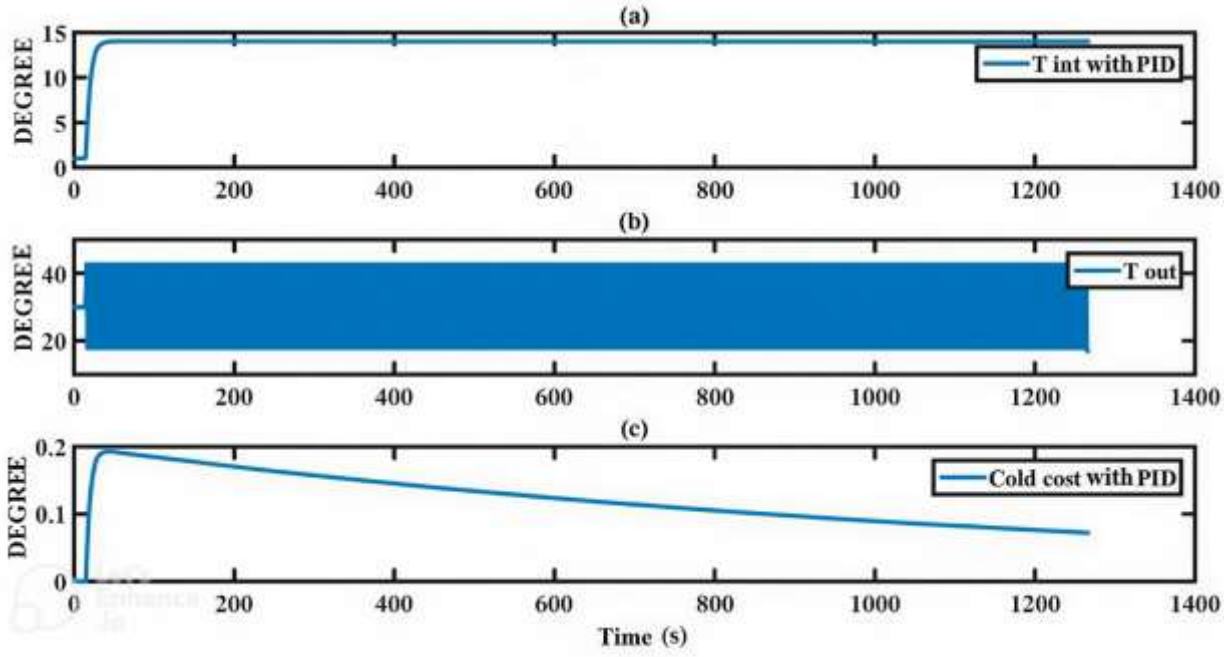

Figure 12: *Experience 6 [32 °C, 30 °C, 14 °C]*

1.5. Comparative analysis of key curves

Figure 13 illustrates the cooling flow gain as a function of time when the thermostat receives the error signal between the reference temperature and the indoor room temperature. This feedback enables system regulation to maintain the comfort temperature at all times, despite the slow response time.

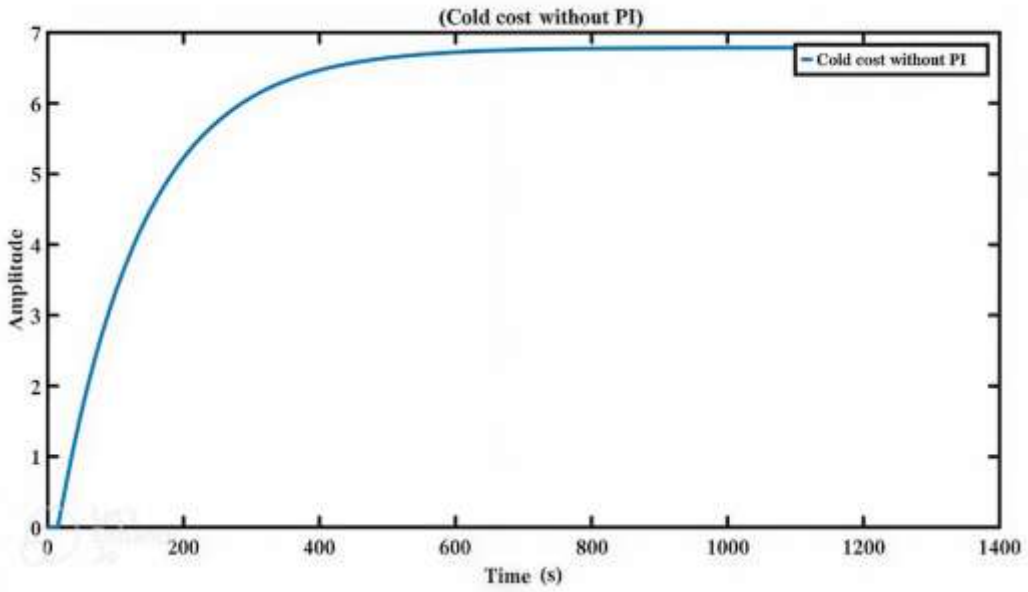

Figure 13: *Cold flow cost or gain curve without PID*

Figure 14 highlights the indoor temperature profile as a function of time, independent of the room's thermal resistance and heat losses. The indoor temperature is set according to the desired comfort level. System regulation ensures that this comfort temperature is maintained at all times, although the response time remains slow
.

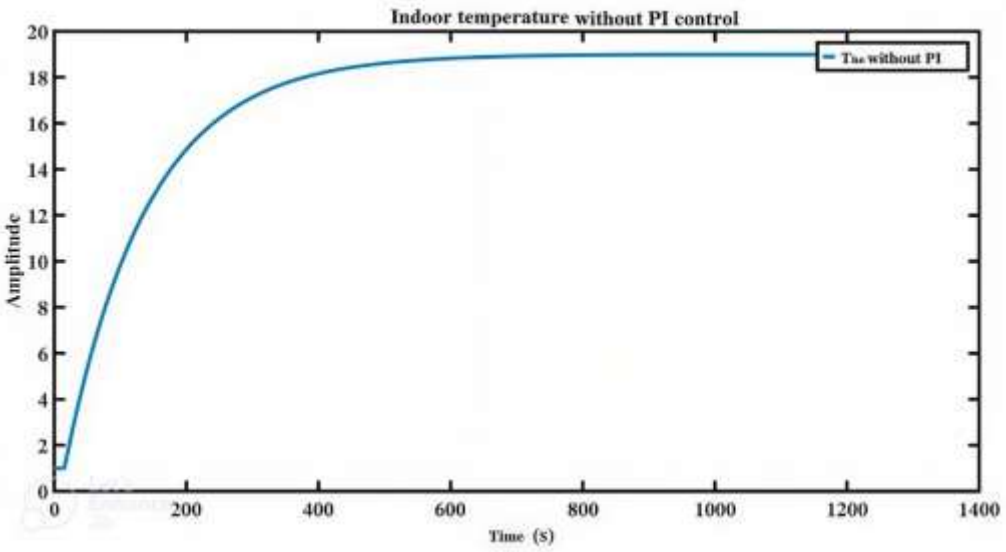

Figure 14*: Indoor Temperature Curve without PID*

The profile of Figure 15 illustrates the outdoor temperature variations across all seasons. It is this annual temperature fluctuation that poses a challenge to the thermal comfort of the dwelling, during both the dry and rainy seasons.

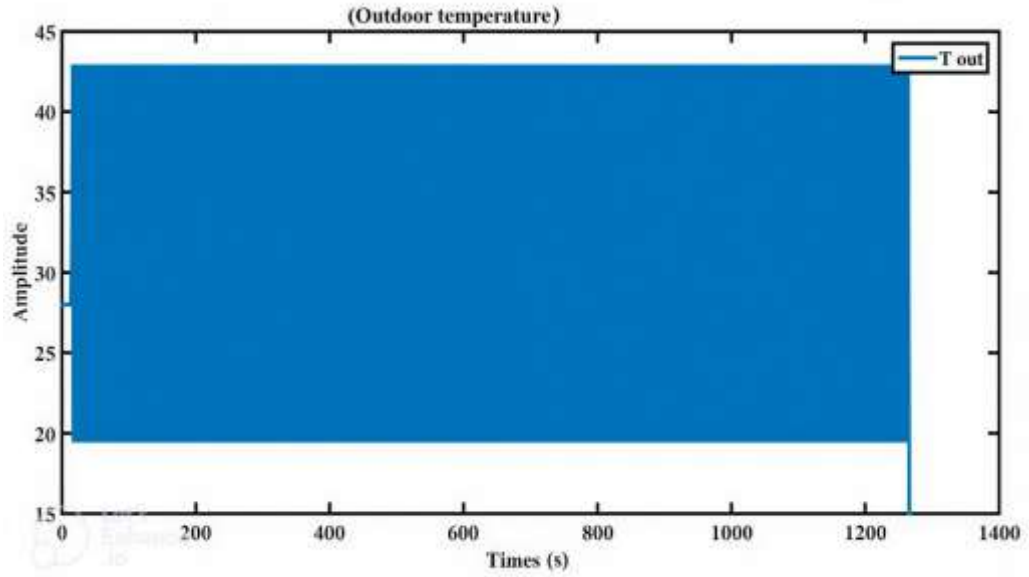

Figure 15: *Outdoor temperature profile*

In the proposed absorption refrigeration system, the gain of the cooling flow, or more generally the efficiency of the refrigerant flow, is illustrated in Figure 16, highlighting its crucial role in the overall system performance.

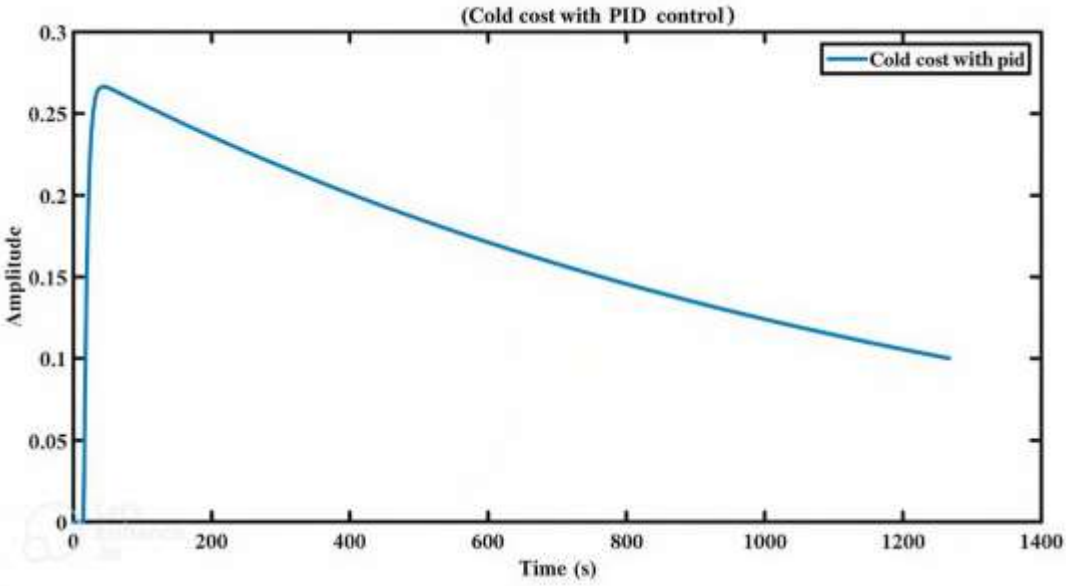

Figure 16: *Curve of the cooling flow cost or gain with PID*

Figure 17 presents the indoor temperature response with PID control. The initial rise time is approximately 400 s prior to the implementation of the PID controller. After tuning the PID, the system response time is reduced to approximately 59 s. The target comfort temperature is set at 19 °C. Under these conditions, the moment at which the system reaches stability can be observed. Several stages are considered to analyze the system performance:

• **Rise time:**

Before adding the controller, the system required approximately 400 s to transition from the initial temperature to a value close to the setpoint (e.g., 90% of the target value). After tuning with the PID controller, the rise time is significantly improved to approximately 59 s.

• Response time:

The response time corresponds to the duration required for the system output to reach and remain close to the setpoint within an acceptable error margin (±5% of the reference value). In this case, following the implementation of the PID controller, the system reaches the comfort temperature of 19 °C in 59 s.

- **Stabilization:**

System stabilization indicates the moment when the temperature no longer fluctuates beyond the defined tolerance (±5% of 19 °C, i.e., between 18.05 °C and 19.95 °C). Beyond this point, the system no longer overshoots and remains within the tolerance band. The settling time is typically defined as the time at which the system ceases to oscillate and remains within this tolerance for the remainder of the observation.

- **Estimation of the stabilization period:**

Given that the response time is 59 s, the system reaches the comfort temperature of 19 °C in less than one minute. However, for the system to be fully stable, exhibiting minimal oscillations and a steady response, the settling time may vary slightly depending on the PID tuning. Nevertheless, it is likely to remain close to 59 s if the PID parameters are well optimized.

In summary, with a response time of 59 s, the system is expected to stabilize shortly after this delay, (probably within a few additional seconds), and to maintain the comfort temperature of 19 °C within the acceptable tolerance range.

Reducing response time is practically important because it allows the cooling system to reach the desired comfort temperature more quickly and maintain it with less delay when outdoor conditions changes. In real buildings, this means fewer periods of discomfort, better control during occupancy peaks, less temperature fluctuation, and improved overall reliability of the cooling system.

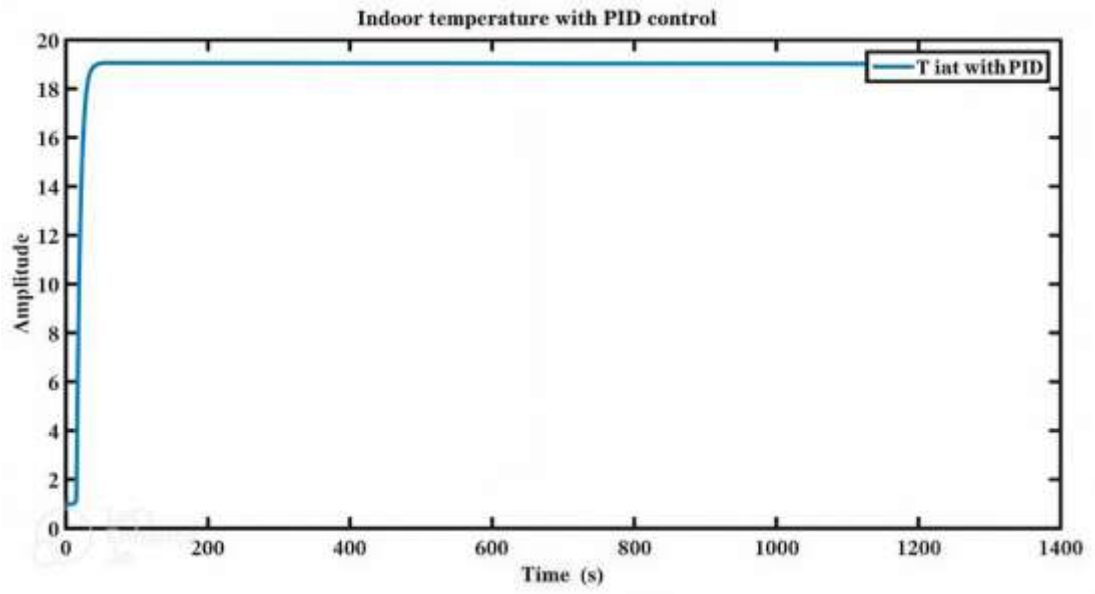

Figure 17: *Indoor Room Temperature Curve with PID Control*

1.6. PID controller performance

Figure 18 illustrates the system response with the PID controller applied to a first-order system with $K_p = 25$, $K_i = 0.0025$, and $K_d = 0$. It can be observed that the PID controller is a powerful tool for enhancing the performance of a control system. The three terms — proportional, integral, and derivative — act together to reduce the error, eliminate steady-state error, and stabilize the response. Through mathematical modeling, it is possible to predict and fine-tune the system's behavior.

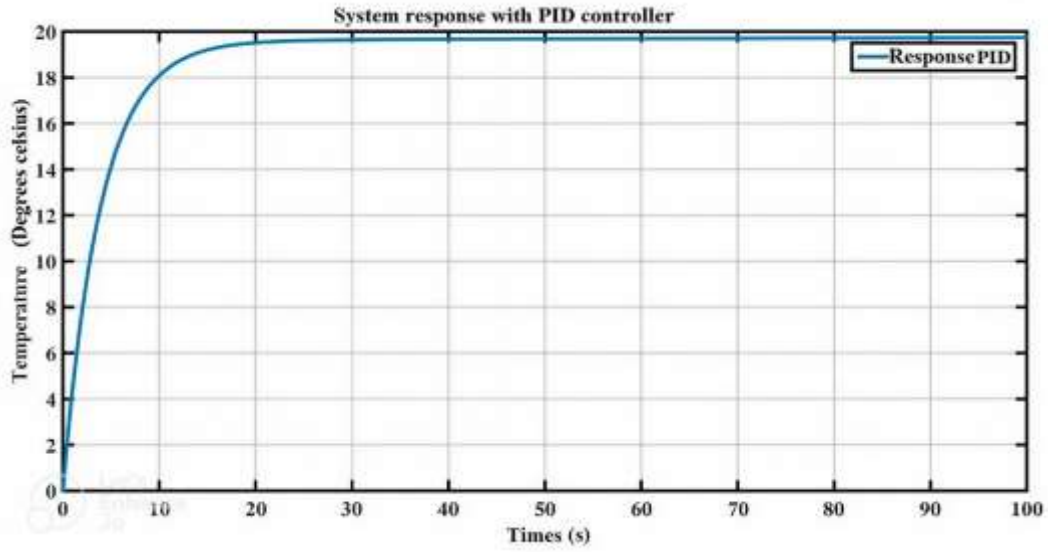

Figure 18. *System Response Curve with PID (First-Order System)*

Figure 19 illustrates the system response with a PID controller using the following control parameters: $K_p = 25$, $K_i = 0.0025$, and $K_d = 0$. The system is assumed to be of second order, with a transfer function of the form $G(s) = 1/(s^2 + \xi\omega_n s)$ in closed-loop configuration.

In the Laplace domain, G(s) represents the transfer function of the thermal process linking the controller input to the room temperature response. In this relation, ξ denotes the damping ratio, ω_n is the natural frequency and (s) is the complex Laplace variable. The parameter $\omega_n$determines the speed of the dynamic response, while ξ governs the degree of oscillation and stability of the response. For ξ < 1, the system is underdamped and exhibits oscillatory behavior; for ξ= 1, it is critically damped; and for ξ > 1, it is overdamped.

The system is subjected to a setpoint change (target temperature of 19 °C), and its response is plotted over an interval of 100 seconds. We observed the temperature response of the absorption refrigeration system after tuning the PID controller, and the parameters were adjusted according to the achieved performance. It can be concluded that the system stabilizes rapidly after a few oscillations around the setpoint value (19 °C), which corresponds to the desired comfort temperature.

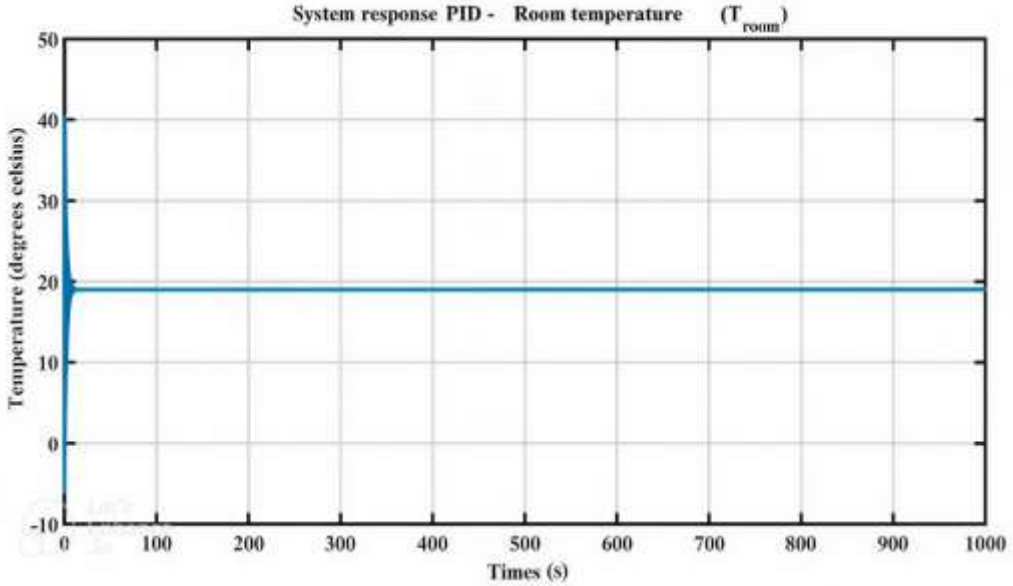

Figure 19. *System Response Curve with PID (Second-Order System)*

3.7 Model validation

Model validation was carried out by comparing (Table 4) the calculated cooling loads with a standard HVAC heat-balance method and by checking the predicted SAR COP against published experimental values for single-effect H_2O-LiBr systems. The cooling loads estimate was found to be consistent with conventional design calculations, which supports the reliability of the load assessment procedure. In addition, the simulated COP falls within the range reported in the literature for comparable solar absorption chillers, indicating that the thermodynamic model produces realistic performance values.

3.8. Limitations, uncertainties, and applicability to other buildings

Although the proposed SAR-PID system performs well for the Ebolowa conference room, several limitations and uncertainties should be acknowledged. First, the performance estimates are based on design conditions and simplified steady-state assumptions, so real operation may differ because of occupant variability, internal load fluctuations, imperfect component behavior, and control uncertainty. The applicability of the results to other buildings will depend on factors such as room geometry, envelope properties, occupancy density, ventilation patterns, and local climate conditions, meaning that the sizing and control strategy should be re-evaluated for each case. In practice, solar intermittency remains a major constraint because short-term fluctuations in irradiance can reduce generator heat supply and affect cooling stability, while rainy-season conditions may further lower collector output and reduce system capacity during periods of high humidity and cloud cover. From an economic standpoint, the initial capital cost of solar collectors, absorption equipment, heat exchangers, and control systems may be higher than that of conventional air-conditioning, although this can be offset over time by reduced electricity consumption and lower operating costs. In addition, LiBr–water absorption systems require careful maintenance, including leak prevention, solution concentration control, corrosion management, vacuum tightness, and crystallization avoidance, all of which are essential for reliable long-term operation.

4. CONCLUSION

This study aimed to enhance thermal comfort in buildings located in humid tropical climates using a SAR system. Through a methodological approach combining thermal load assessment, thermodynamic modeling, and dynamic simulation with PID control, the research demonstrated the technical feasibility and performance of the proposed system. Results indicated that the conference room in Ebolowa requires a cooling capacity of 30.32 kW, which is met by a SAR system with a COP of 0.7, powered by 44 solar thermal panels. The integration of a PID controller reduced the temperature stabilization time from 400 s to 59 s, ensuring rapid and stable thermal comfort under varying external conditions. Exergetic analysis confirmed the system's thermodynamic efficiency. These findings demonstrate that the system can maintain comfortable indoor temperatures in highly heat-exposed environments, such as conference rooms, by relying on renewable resources while limiting dependence on conventional energy sources.

The study also revealed the need to optimize certain system parameters, such as solar collector performance and thermal dissipation management, to achieve maximum efficiency. This research indicates that the adoption of SAR systems could represent a significant advancement for infrastructures in tropical regions of Cameroon, particularly for collective or professional buildings with high cooling demands. It thus stands as a promising alternative to conventional air-conditioning systems, contributing not only to energy cost reduction but also to environmental protection.

In summary, the large-scale implementation of this technology, coupled with policy incentives and subsidies to encourage renewable energy use, could play a pivotal role in Cameroon's energy transition and in improving building thermal comfort. Solar absorption refrigeration represents a sustainable and effective alternative to conventional cooling systems in sun-rich regions. Future work should focus on cost-benefit analysis, long-term performance monitoring, and system optimization for different building types and climatic zones.

Statements and Declarations:

Acknowledgments: The authors are grateful to the Director of ISABEE for authorizing this study within his institution.

Author's contributions:

- Edouard MBOUMBOUE: Conceptualization, Methodology, Formal analysis, Investigation, Writing – Original Draft, Writing – Review & Editing, Project administration, Supervision.
- Clément ONDOUA BELIBI: Methodology, Investigation, Data curation, Validation, Writing – Review & Editing.
- Fabrice KWEFEU MBAKOP: Methodology, Investigation, Software, Visualization.
- Deli GORON: Formal analysis, Exergetic analysis, Validation, Writing – Review & Editing.
- Elvis WATI: Investigation, Validation, Data collection, Writing – Review & Editing.
- Armand CHEDOP: Methodology, Investigation, Writing – Review & Editing.

• Jean Benjamin BIDIAS: Formal analysis, Simulation analysis, Writing – Review & Editing.
• Inoussah MOUNGNUTOU MFETOUM: Conceptualization, Methodology, Supervision, Writing – Review & Editing.

Competing interest: The authors declare that there is no conflict of interest regarding the publication of this paper.

Funding: This research did not receive any specific grants from funding agencies in the public, commercial, or not-for-profit sectors.

REFERENCES

[1] F. Birol, “The Future of Cooling,” International Energy Agency (IEA), 2018.

[2] A. Marcinkowski and D. Levchenko, ‘Comparative Life Cycle Analysis for Duct Air Conditioning Systems Based on Evaporative and Vapor Compression Technologies’, *Energies*, vol. 18, no. 13, p. 3475, Jul. 2025, DOI: 10.3390/en18133475.

[3] B. Bandyopadhyay and M. Banerjee, ‘Decarbonization of cooling of buildings’, *Sol. Compass*, vol. 2, p. 100025, Aug. 2022, DOI: 10.1016/j.solcom.2022.100025.

[4] S. A. M. Said, M. A. I. El-Shaarawi, and M. U. Siddiqui, ‘Alternative designs for a 24-h operating solar-powered absorption refrigeration technology’, *Int. J. Refrig.*, vol. 35, no. 7, pp. 1967–1977, Nov. 2012, doi: 10.1016/j.ijrefrig.2012.06.008.

[5] X. Q. Zhai, M. Qu, Y. Li, and R. Z. Wang, ‘A review for research and new design options of solar absorption cooling systems’, *Renew. Sustain. Energy Rev.*, vol. 15, no. 9, pp. 4416–4423, Dec. 2011, doi: 10.1016/j.rser.2011.06.016.

[6] S. Oubourhim, M. Mmadi Hassane, Y. Filali Baba, A. Al Mers, A. Kheiri, and O. Botella, ‘Literature review on advancements in solar absorption refrigeration for sustainable cooling systems,’ *EPJ Web Conf.*, vol. 326, p. 04002, 2025, doi: 10.1051/epjconf/202532604002.

[7] A. Saleh and M. Mosa, ‘Optimization study of a single-effect water–lithium bromide absorption refrigeration system powered by flat-plate collector in hot regions’, *Energy Convers. Manag.*, vol. 87, pp. 29–36, Nov. 2014, DOI: 10.1016/j.enconman.2014.06.098.

[8] A. Syed *et al.*, ‘A novel experimental investigation of a solar cooling system in Madrid’, *Int. J. Refrig.*, vol. 28, no. 6, pp. 859–871, Sep. 2005, DOI: 10.1016/j.ijrefrig.2005.01.007.

[9] C. Çetiner, ‘Thermal analysis of operating a solar-powered diffusion absorption refrigerator with a parabolic collector’, *Case Stud. Therm. Eng.*, vol. 53, p. 103893, Jan. 2024, DOI: 10.1016/j.csite.2023.103893.

[10] Y. Bi, L. Qin, J. Guo, H. Li, and G. Zang, ‘Performance analysis of solar air conditioning system based on the independent-developed solar parabolic trough collector’, *Energy*, vol. 196, p. 117075, Apr. 2020, doi: 10.1016/j.energy.2020.117075.

[11] X. Zhang, H. Li, and C. Yang, ‘A novel solar absorption refrigeration system using the multi-stage heat storage method’, *Energy Build.*, vol. 102, pp. 157–162, Sep. 2015, doi: 10.1016/j.enbuild.2015.05.011.

[12] S. Rosiek and F. J. Batlles, ‘Integration of the solar thermal energy in the construction: Analysis of the solar-assisted air-conditioning system installed in CIESOL building’, *Renew. Energy*, vol. 34, no. 6, pp. 1423–1431, Jun. 2009, doi: 10.1016/j.renene.2008.11.021.

[13] J. Fitó, S. Mauran, D. Stitou, N. Mazet, and A. Coronas, ‘New solar hybrid absorption / thermochemical refrigeration cycle,’ in *Proc. Int. Conf. on Solar Heating and Cooling for Buildings and Industry*, 2015

[14] J. Fitó, A. Coronas, S. Mauran, N. Mazet, and D. Stitou, ‘Definition and performance simulations of a novel solar-driven hybrid absorption-thermochemical refrigeration system’, *Energy Convers. Manag.*, vol. 175, pp. 298–312, Nov. 2018, doi: 10.1016/j.enconman.2018.08.098.

[15] C. Blackman and C. Bales, ‘Experimental evaluation of a novel absorption heat pump module for solar cooling applications’, *Sci. Technol. Built Environ.*, vol. 21, no. 3, pp. 323–331, Apr. 2015, doi: 10.1080/10789669.2014.990336.

[16] M. M. A. Khan, R. Saidur, and F. A. Al-Sulaiman, ‘A review for phase change materials (PCMs) in solar absorption refrigeration systems’, *Renew. Sustain. Energy Rev.*, vol. 76, pp. 105–137, Sep. 2017, doi: 10.1016/j.rser.2017.03.070.

[17] H. Zhu, B. Guo, W. Geng, J. Chi, and S. Guo, ‘Simulation of an improved solar absorption refrigeration system with phase change materials’, *Energy Rep.*, vol. 8, pp. 3671–3679, Nov. 2022, DOI: 10.1016/j.egyr.2022.02.306.

[18] R. Hirmiz, M. F. Lightstone, and J. S. Cotton, ‘Performance enhancement of solar absorption cooling systems using thermal energy storage with phase change materials’, *Appl. Energy*, vol. 223, pp. 11–29, Aug. 2018, DOI: 10.1016/j.apenergy.2018.04.029.

[19] H. Ma *et al.*, 'Operating performance and economic analysis of solar single/double-effect compound absorption refrigeration system', *Sol. Energy*, vol. 247, pp. 73–85, Nov. 2022, DOI: 10.1016/j.solener.2022.10.005.

[20] M. S. A. Khan, A. W. Badar, T. Talha, M. W. Khan, and F. S. Butt, 'Configuration based modeling and performance analysis of single effect solar absorption cooling system in TRNSYS', *Energy Convers. Manag.*, vol. 157, pp. 351–363, Feb. 2018, doi: 10.1016/j.enconman.2017.12.024.

[21] R. Mansouri, M. Bourouis, and A. Bellagi, 'Experimental investigations and modeling of a small capacity diffusion-absorption refrigerator in dynamic mode', *Appl. Therm. Eng.*, vol. 113, pp. 653–662, Feb. 2017, DOI: 10.1016/j.applthermaleng.2016.11.078.

[22] J. Freeman and C. N. Markides, 'A solar diffusion-absorption refrigeration system for off-grid cold-chain provision, Part II: System simulation and assessment of performance', *Renew. Energy*, vol. 230, p. 120717, Sep. 2024, DOI: 10.1016/j.renene.2024.120717.

[23] J. López-Villada, D. S. Ayou, J. C. Bruno, and A. Coronas, 'Modeling, simulation and analysis of solar absorption power-cooling systems', *Int. J. Refrig.*, vol. 39, pp. 125–136, Mar. 2014, doi: 10.1016/j.ijrefrig.2013.11.004.

[24] S. A. M. Said, M. A. I. El-Shaarawi, and M. U. Siddiqui, 'Intermittent absorption refrigeration system equipped with an economizer', *Energy*, vol. 61, pp. 332–344, Nov. 2013, doi: 10.1016/j.energy.2013.09.034.

[25] H. Yuan, J. Zhang, X. Huang, and N. Mei, 'Experimental investigation on binary ammonia–water and ternary ammonia–water–lithium bromide mixture-based absorption refrigeration systems for fishing ships', *Energy Convers. Manag.*, vol. 166, pp. 13–22, Jun. 2018, doi: 10.1016/j.enconman.2018.04.013.

[26] G. Moreno-Quintanar, W. Rivera, and R. Best, 'Comparison of the experimental evaluation of a solar intermittent refrigeration system for ice production operating with the mixtures NH3/LiNO3 and NH3/LiNO3/H2O', *Renew. Energy*, vol. 38, no. 1, pp. 62–68, Feb. 2012, doi: 10.1016/j.renene.2011.07.009.

[27] M. Jalalizadeh, R. Fayaz, S. Delfani, H. J. Mosleh, and M. Karami, 'Dynamic simulation of a trigeneration system using an absorption cooling system and building integrated photovoltaic thermal solar collectors', *J. Build. Eng.*, vol. 43, p. 102482, Nov. 2021, doi: 10.1016/j.jobe.2021.102482.

[28] A. Shirazi, S. Pintaldi, S. D. White, G. L. Morrison, G. Rosengarten, and R. A. Taylor, 'Solar-assisted absorption air-conditioning systems in buildings: Control strategies and operational modes', *Appl. Therm. Eng.*, vol. 92, pp. 246–260, Jan. 2016, doi: 10.1016/j.applthermaleng.2015.09.081.

[29] S. Noferesti, M. Ahmadzadehtalatapeh, and V. G. Motlagh, 'The application of solar integrated absorption cooling system to improve the air quality and reduce the energy consumption of the air conditioning systems in buildings – A full year model simulation', *Energy Build.*, vol. 274, p. 112420, Nov. 2022, doi: 10.1016/j.enbuild.2022.112420.

[30] F. Reda, M. Viot, K. Sipilä, and M. Helm, 'Energy assessment of solar cooling thermally driven system configurations for an office building in a Nordic country', *Appl. Energy*, vol. 166, pp. 27–43, Mar. 2016, doi: 10.1016/j.apenergy.2015.12.119.

[31] J. Aman, D. S.-K. Ting, and P. Henshaw, 'Residential solar air conditioning: Energy and exergy analyses of an ammonia–water absorption cooling system', *Appl. Therm. Eng.*, vol. 62, no. 2, pp. 424–432, Jan. 2014, DOI: 10.1016/j.applthermaleng.2013.10.006.

[32] E. D. Kerme, A. Chafidz, O. P. Agboola, J. Orfi, A. H. Fakeeha, and A. S. Al-Fatesh, 'Energetic and exergetic analysis of solar-powered lithium bromide-water absorption cooling system', *J. Clean. Prod.*, vol. 151, pp. 60–73, May 2017, doi: 10.1016/j.jclepro.2017.03.060.

[33] Studocu. Etude paramétrique d'un système de réfrigération par absorption, Available online at: https://www.studocu.com/row/document/faculte-des-sciences-semlalia-de-marrakech/s3-mecanique-des-solides/etude-parametrique-dun-systeme-de-refrigeration-par-absorption/156467237. [Last access: Mar. 23, 2026]

[34] Y. Kaita, 'Thermodynamic properties of lithium bromide–water solutions at high temperatures', *Int. J. Refrig.*, vol. 24, no. 5, pp. 374–390, Aug. 2001, doi: 10.1016/S0140-7007(00)00039-6.

[35] V. V. Patel, 'Ziegler-Nichols Tuning Method: Understanding the PID Controller', *Resonance*, vol. 25, no. 10, pp. 1385–1397, Oct. 2020, doi: 10.1007/s12045-020-1058-z.

[36] H. A. Al-Tahaineh, 2023. "Exergetic-energetic effectiveness of a simple H_2O-LiBr absorption chiller operated by solar energy collected using a direct flow evacuated tube collector", *International Journal of Low-Carbon Technologies*, Oxford University Press, vol. 18, pages 689-696.

[37] A. A. O. Villa, J. C. C. Dutra, and J. R. H. Guerrero, 2014. "Energy and exergy analysis of the performance of

10 TR lithium bromide/water absorption chiller", *Rev. Téc. Ing. Univ. Zulia,* vol. 37 n^0 1 Maracaibo abr. 2014.

[38] A. Zendehnam and F. Pourfayaz, 2022. "Sensitivity analysis of avoidable and unavoidable exergy destructions in a parallel double-effect LiBr-water absorption cooling system", *Energy Sci. Eng*.2023; 11:527-546. DOI: 10.1002/ese3.1344.

[39] J. Zheng, J. Castro, A. Oliva, and C. Oliet, (2021). "Energy and exergy analysis of an absorption system with working pairs LiBr-H_2O and Carrol-H_2O at applications of cooling and heating", *International Journal of Refrigeration*, 132 (2021) 156-171. https://doi.org/10.1016/j.ijrefrig.2021.09.011